

Chaotic dynamics of Pr^{3+}/Yb^{3+}-doped all-fiber up-conversion visible fiber laser

Yisong Li(李义松), Yueling Hao(郝悦伶), Juanfen Wang(王娟芬), Xiaohui Chen(陈晓晖), Shengxiang Chen(陈胜祥), Chao Zhou(周超), Lingzhen Yang(杨玲珍)

Citation: Chin. Phys. B, 2026, 35 (**1**): 014208. DOI: 10.1088/1674-1056/ade4b5
http://cpb.iphy.ac.cn; http://iopscience.iop.org/cpb

What follows is a list of articles you may be interested in

Stability, bifurcation, chaotic pattern, phase portrait and exact solutions of a class of semi-linear Schr?dinger equations with Kudryashov's power law self-phase modulation and multiplicative white noise based on Stratonvich's calculus

Cheng-Qiang Wang(王成强), Xiang-Qing Zhao(赵向青), Yu-Lin Zhang(张玉林), and Zhi-Wei Lv(吕志伟)
Chin. Phys. B, 2025, 34 (**12**): 124205. DOI: 10.1088/1674-1056/ade664

Real-time observations of the transition dynamics between multiple nonlinear states in a coherently driven Kerr fiber-loop resonator

Yayu Cao(曹亚昱), Heng Dong(董恒), and Xiankun Yao(姚献坤)
Chin. Phys. B, 2025, 34 (**7**): 074206. DOI: 10.1088/1674-1056/adc40a

Polarization-sensitive nonlinear optical diffraction

Jianluo Chen(陈健洛), Lihong Hong(洪丽红), Yu Zou(邹娱), Jiacheng Li(李嘉诚), and Zhi-Yuan Li(李志远)
Chin. Phys. B, 2025, 34 (**6**): 064204. DOI: 10.1088/1674-1056/adc401

Pure-quartic soliton molecules in normal fourth-order dispersion regimes based on spectral filtering effect

Han-Yang Shen(申翰阳), Rui-Bo Lan(蓝睿博), Hong-Bin Hu(胡洪彬), Yang Li(李阳), Rui Zhou(周瑞), and Zu-Xing Zhang(张祖兴)
Chin. Phys. B, 2025, 34 (**3**): 034203. DOI: 10.1088/1674-1056/ada43c

Dissipative soliton resonance within different dispersion regimes in a single mode-locked laser

Zhetao Zhao(赵哲韬), Qinke Shu(舒沁珂), Ziyi Xie(解梓怡), Yuxuan Ren(任俞宣), Ying Zhang(张颖), Bo Yuan(袁博), Chunbo Zhao(赵春勃), Junsong Peng(彭俊松), and Heping Zeng(曾和平)
Chin. Phys. B, 2024, 33 (**7**): 074208. DOI: 10.1088/1674-1056/ad47b1

Chaotic dynamics of Pr^{3+}/Yb^{3+}-doped all-fiber up-conversion visible fiber laser

Yisong Li(李义松)[1,†], Yueling Hao(郝悦伶)[1,†], Juanfen Wang(王娟芬)[1], Xiaohui Chen(陈晓晖)[1], Shengxiang Chen(陈胜祥)[1], Chao Zhou(周超)[1], and Lingzhen Yang(杨玲珍)[1,2,‡]

[1] *College of Physics and Optoelectronics, Taiyuan University of Technology, Taiyuan* 030024, *China*
[2] *Laboratory of Advanced Transducers and Intelligent Control System, Ministry of Education, Taiyuan University of Technology, Taiyuan* 030024, *China*

(Received 19 April 2025; revised manuscript received 7 June 2025; accepted manuscript online 16 June 2025)

We investigate theoretically and experimentally the chaotic dynamics of visible-wavelength all-fiber ring laser. The 100-m 630 HP fibers are used to ensure high non-linearity. A 4-m Pr^{3+}/Yb^{3+}-co-doped ZBLAN fiber provides the gain. The chaotic laser was pumped by the laser diodes with the maximum power of 150 mW at the wavelength of 850 nm. The peak fluorescence spectrum of Pr^{3+}/Yb^{3+}-co-doped ZBLAN fiber at the wavelength of 635 nm shows that the visible-wavelength fiber laser can be achieved by synergistic energy transfer between Pr^{3+} and Yb^{3+} ions. The chaotic fiber laser is generated by adjusting the pump power, polarization controller and the auto-correlation, permutation entropy, skewness, and kurtosis were used to analyze the characteristics of chaotic laser. The noise-like time series and delta-like auto-correlation curve indicate the chaotic output. The complexity and randomness of time series are analyzed by the permutation entropy, skewness, and kurtosis. The result shows that chaotic dynamics is stable when the pump power exceeds a certain value. The visible chaotic all-fiber laser has high stability and can be applied for real-time monitoring and sensing. We believe that this approach may also be feasible for other materials for emission in the visible range.

Keywords: chaotic lasers, visible fiber laser, randomness, Pr^{3+}/Yb^{3+} doped fiber

PACS: 42.65.Sf, 42.60.–v, 42.55.Wd, 05.45.–a

DOI: 10.1088/1674-1056/ade4b5 **CSTR:** 32038.14.CPB.ade4b5

1. Introduction

Chaotic laser has the characteristics of randomness,[1] broad bandwidth,[2] delta-like auto-correlation curve,[3] and the anti-interference capability.[4] They are applied in numerous fields, including the chaotic secure communications,[5,6] generation of random numbers,[7–9] optical fiber sensing,[10,11] and chaotic lidar.[12,13] Semiconductor laser can achieve the output of chaotic light through external optical injection,[14] optical feedback,[15] and optoelectronic feedback.[16,17] For fiber laser, the nonlinear effect of optical fibers can be exploited to realize the generation of chaotic laser.[3] Over the past few decades, chaotic fiber laser in the near-infrared spectral region have been applied for sensing and imaging.[18] The 1550-nm chaotic laser can achieve a spatial resolution of 10 cm across a sensing distance of 1.4 km. This method can enhance the spatial resolution by a factor of 50.[19]

The visible-wavelength fiber lasers exploit the unique spectral properties and superior transmission characteristics and have applications due to its notable performance in a wide variety of industries.[20] In the past two decades, the rapid development of low-loss rare-earth-doped (such as Pr^{3+}, Dy^{3+}, and Ho^{3+}) ZBLAN (ZrF_4–BaF_2–LaF_3–AlF_3–NaF) fibers,[21–24] high-power blue gallium nitride laser diode (GaN-LD),[25] and proposal of up-conversion pumping scheme (via pumping by a near infrared wavelengths) have promoted the development of all-fiber lasers for the visible wavelength.[26] The Pr^{3+}/Yb^{3+}-co-doped ZBLAN fiber enables up-conversion luminescence in Pr^{3+} ions, with Yb^{3+} serving as an efficient sensitizer due to its strong energy transfer capabilities. In a free-space cavity configuration, researchers achieved an 8-mW continuous-wave blue light output by employing a 30-cm segment of Pr^{3+}/Yb^{3+}-co-doped ZBLAN fiber, pumped by an 850-nm laser source with a power of 200 mW.[27] Researchers demonstrated the generation of 65-ps dissipative soliton pulses at 635 nm using a 3.5-m Pr^{3+}/Yb^{3+}-co-doped ZBLAN fiber, enabled by the up-conversion mechanism and mode-locked via a nonlinear amplifying loop mirror.[28] In recent years, fiber lasers in the visible wavelength have demonstrated the output of high-power continuous-wave lasers,[29,30] Q-switched lasers,[31,32] and ultrashort-pulse lasers.[33–35]

This paper demonstrates a visible-wavelength chaotic all-fiber laser. We numerically predicted the evolution of chaos in the Pr^{3+}/Yb^{3+} co-doped fiber laser. The chaotic laser with a wavelength of 635 nm was experimentally generated by incorporating a certain length of single-mode fiber into the fiber ring cavity to enhance the nonlinear effect. Its time series exhibits a delta-like characteristics of auto-correlation curve. The ex-

[†]The two authors contributed equally to this work.
[‡]Corresponding author. E-mail: office-science@tyut.edu.cn
© 2026 Chinese Physical Society and IOP Publishing Ltd. All rights, including for text and data mining, AI training, and similar technologies, are reserved.

perimental results are in excellent agreement with the numerical results. The 635-nm chaotic laser demonstrates the potential application in skincare, biomedical sensing, and high-precision imaging.

2. Numerical analysis

The models for generating chaos in fiber lasers include parameter modulation,[36] optical delayed feedback, dual-ring coupling, nonlinear fiber loop mirror, and nonlinear Kerr effect.[37] The energy-level lifetime of doped ions impacts the bandwidth of chaotic laser. By increasing the length of ring cavity to enhance the intracavity nonlinear Kerr effect for chaotic generation, the method can avoid the influence of doped ions and it can generate chaotic lasers with broader bandwidth and achieve chaotic lasers with GHz-level bandwidth. This paper adopts the nonlinear Kerr effect to generate chaotic lasers in fiber lasers. By adjusting the polarization controller and pump power, the laser can be driven into a chaotic state. These factors also influence the randomness and complexity of the chaotic laser.

In an optical fiber ring cavity, the optical field is given by $E(z,t) = \varepsilon(z,t)\exp(\mathrm{i}(k_0 z - \omega_0 t))$, where ω_0 represents the optical wave angular frequency. In the relative coordinate $\tau = t - z/v_\mathrm{g}$, with v_g denoting the group velocity, the propagation of the optical field envelope can be characterized as follows:

$$\frac{\partial \mathcal{E}_{x,y}(z,\tau)}{\partial z} = gn(\tau)\mathcal{E}_{x,y} + \boldsymbol{L}_{x,y}\mathcal{E}_{x,y} + \boldsymbol{N}_{x,y}\mathcal{E}_{x,y}, \tag{1}$$

where $\boldsymbol{L}_{x,y}$ is the linear operator for optical field propagation, which includes linear birefringence, group velocity dispersion, and gain dispersion. $\boldsymbol{L}_{x,y}$ is usually expressed in the frequency domain, and its specific expression is

$$L_{x,y} = \pm\frac{\mathrm{i}k_0(n_x - n_y)}{2n_0} + \frac{\Delta}{n_0 c}\mathrm{i}\omega - \frac{\mathrm{i}}{2}\beta_2\omega^2 + \frac{1 - gn(\tau)(1+\omega^2 T_2^2)}{1+\omega^2 T_2^2}. \tag{2}$$

The $\boldsymbol{N}_{x,y}$ is the nonlinear operator for optical field propagation, which is related to the nonlinear Kerr effect and is usually expressed in the spatial domain. Its specific expression is

$$\boldsymbol{N}_{x,y}\varepsilon_{x,y} = \mathrm{i}\gamma\left\{\left(|\varepsilon_{x,y}(z,\tau)|^2 + \frac{2}{3}|\varepsilon_{y,x}(z,\tau)|^2\right) \times \varepsilon_{x,y}(z,\tau)\right\}. \tag{3}$$

A Pr^{3+}/Yb^{3+}-co-doped ZBLAN fiber provides the gain, and the long single-mode fiber improves the nonlinear effect in the cavity. The parameters of each component in the laser cavity are listed in Table 1. The simulation parameters are aligned with the experimental setup. The simulation starts with random Gaussian noise as the initial input.

Table 1. Simulation parameters of the Pr^{3+}/Yb^{3+} ZBLAN fiber.

Parameter	Value	Parameter	Value
L	4 m	γ	66.1 $\mathrm{W^{-1}\cdot km^{-1}}$
Ω_g	4 nm	g	variable
P_sat	0.3 mW	$\tau_{635\ \mathrm{nm}}$	20 μs
λ_s	635 nm	$\sigma_{635\ \mathrm{nm}}$	8.1×10^{-24} $\mathrm{m^2}$
λ_p	850 nm	α_p	4 dB/m
R	95:5	β_2	42.32 $\mathrm{ps^2\cdot km^{-1}}$

We numerically simulated the formation and temporal evolution of chaotic laser dynamics. The single-mode fiber length was fixed at 100 m, while the pump power was varied from 5 mW to 150 mW to investigate the output. The autocorrelation trace of the time series determines whether the output of the laser is chaotic state. The simulation results show the time series of fiber laser at a pump power of 100 mW as shown in Fig. 1. The output of time series is shown in Fig. 1(a) and has the high peak-to-peak amplitude with random fluctuations. The autocorrelation of the time series shown in Fig. 1(b) shows the delta-like autocorrelation trace with a value of 1 at zero delay and a low pedestal. The full width at half maximum (FWHM) of the auto-correlation is measured to be 0.022 ns and it demonstrates the system enter into a chaotic state with strong stochastic properties. The simulation maintains a chaotic output state with the further increases of pump power and demonstrate the robustness of the chaotic dynamics.

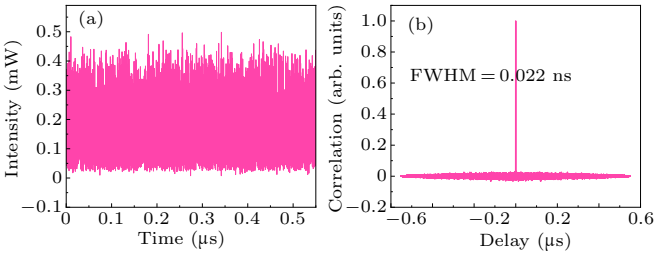


Fig. 1. Simulation results at 100-mW pump power: (a) time series, (b) auto-correlation.

3. Experimental setup

Figure 2 illustrates the experimental setup of the 635-nm all-fiber chaotic laser. The laser utilizes a counter-pumping scheme, and it can improve the power conversion efficiency and system stability. An 850-nm laser diode (LD) with a single-mode fiber is utilized to pump the ZBLAN fiber through a 635/850-nm wavelength division multiplexer (WDM). The setup consists of a 4-m Pr^{3+}/Yb^{3+}-co-doped ZBLAN fiber, an inline fiber polarization controller (PC) to adjust the polarization state in the ring cavity, and a 100-m 630 HP single-mode fiber to enhance the nonlinear effects within the cavity. The Pr^{3+}/Yb^{3+}-co-doped ZBLAN fiber (ZSF SM [0.78], Pr^{3+} 3000 ppm, Yb^{3+} 20000 ppm) exhibits an absorption coefficient of approximately 4.0 dB/m at 850 nm, and enable the efficient up-conversion gain at 635 nm through synergistic energy transfer (ET) between Pr^{3+} and Yb^{3+} ions.

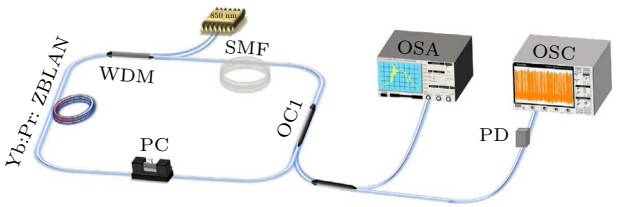


Fig. 2. Experimental setup of the 635-nm chaotic laser system.

Figure 3 shows the Pr^{3+}/Yb^{3+}-co-doped ZBLAN fiber pumped with an 850-nm laser at 150 mW. It can be observed that the emission peak at 635 nm is the strongest. The emission peaks are also observed at 603 nm, 491 nm, 716 nm, and 520 nm. This indicates that the Pr^{3+}/Yb^{3+}-co-doped ZBLAN fiber is capable of achieving laser output in other visible wavelength.

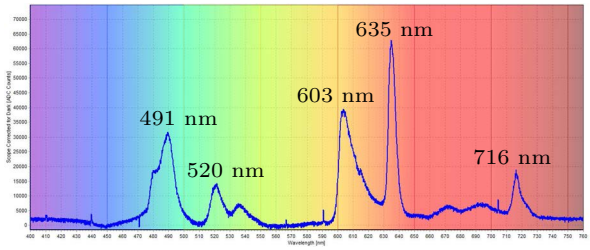


Fig. 3. Fluorescence spectrum of Pr^{3+}/Yb^{3+}-co-doped fluoride fiber pumped with an 850-nm laser at 150 mW.

In addition, we fabricated Pr^{3+}/Yb^{3+}-co-doped ZBLAN fiber patch cords and efficiently connected them to single-mode silicate 630 HP fibers via fiber adapters. By adjusting the pump current and PC, nonlinear effects in the ring cavity can be controlled. The chaotic laser passing through the OC1 with a splitting ratio of 95:5, 95% of the signal light continues to circulate in the cavity, and 5% of the signal light is output through the output port. The output spectrum was measured using a 190 nm–1100 nm optical spectrum analyzer (OSA, Avasoft) and the resolution of the OSA is 0.05 nm. The time series of chaotic laser are recorded by the oscilloscope (OSC, Tektronix MSO64) with 2.5-GHz bandwidth.

4. Result and discussion

In the experiment, the threshold of the fiber laser is 75 mW. When the pump power exceeds 75 mW, a stable laser can be observed. As shown in Fig. 4(a), the maximum output power is 128 μW, and the output power increases linearly with the pump power, and the inset of Fig. 4(a) shows the color of the red laser on the color card. Figure 4(b) shows the spectrum of chaotic laser at a pump power of 150 mW, and it can be seen that the center wavelength is 635.04 nm and the 3-dB bandwidth is 1.21 nm. Figure 4(c) plots a typical chaotic sequence with high peak-to-peak values and the output with the noise-like time series indicate that the chaotic laser is very stable. The inset of Fig. 4(c) is the delta-like characteristics of autocorrelation curve and the autocorrelation curve demonstrates that the laser has entered a chaotic state, figure 4(d) displays the frequency spectrum of the chaotic laser and exhibit broadband spectral properties with a bandwidth of 2.5 GHz. The recorded spectrum is limited by the photodetector and oscilloscope.

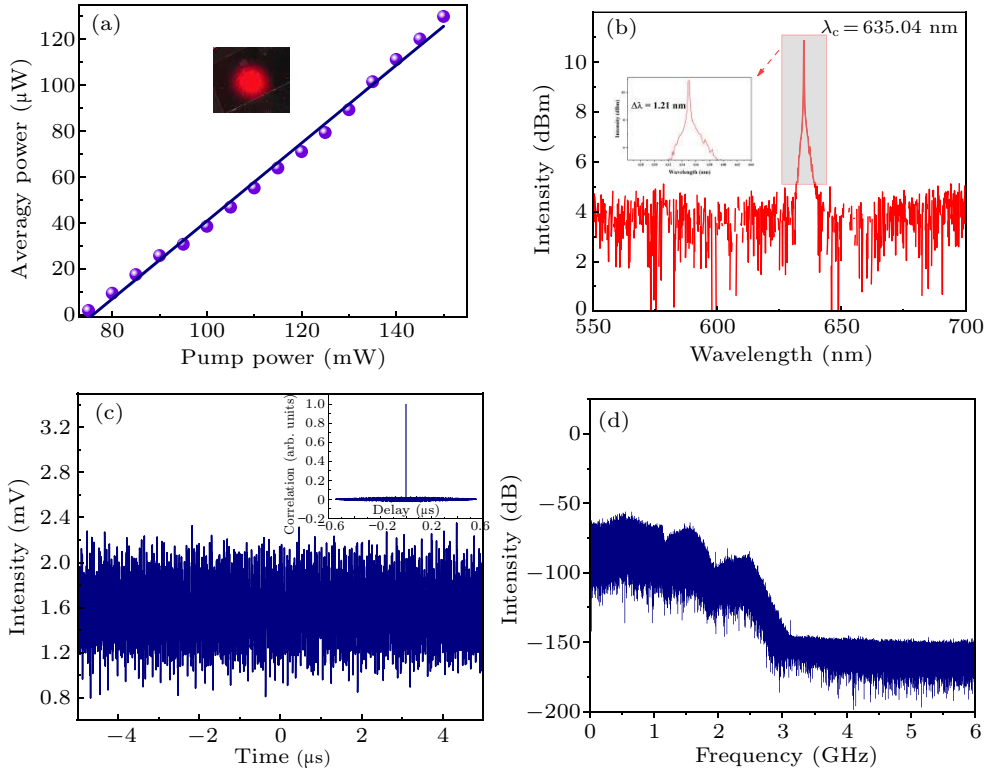


Fig. 4. The output of the visible-wavelength chaotic fiber laser under a pump power of 150 mW: (a) average output power *versus* pump power, (b) optical spectrum, (c) time series, (d) frequency spectrum.

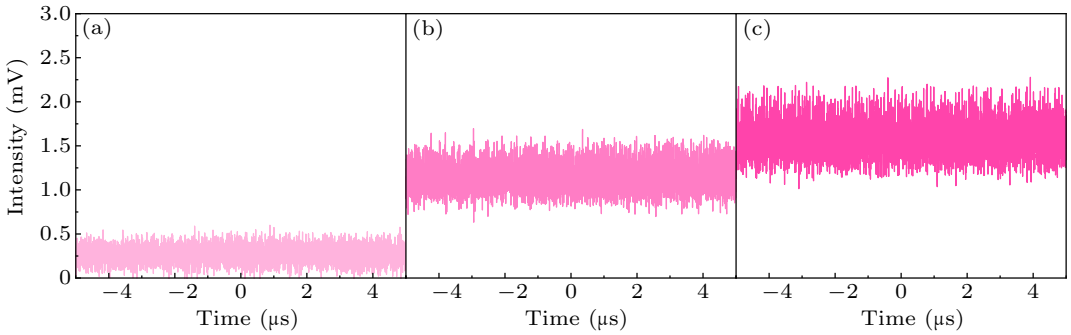


Fig. 5. The time series of chaotic laser output under different pump powers: (a) 90 mW, (b) 130 mW, (c) 150 mW.

The output of the chaotic laser at different powers is shown in Fig. 5. It can be seen from Fig. 5 that both the average voltage and the peak-to-peak values of the time series of the chaotic laser increase with the increases of pump power. When the pump power is 150 mW, the peak-to-peak value reaches 1.2 mV. A higher peak-to-peak value can effectively enhance the randomness of the chaotic laser.

To achieve the chaotic time series with high complexity and randomness, the complexity and statistical properties of the time series of chaotic laser at difference pump power are analyzed shown in Fig. 6. Figure 6(a) shows the permutation entropy of the chaotic laser with the pump power and it can be seen that the permutation entropy of the chaotic laser is stable between 110 mW and 150 mW. The skewness and kurtosis are used to further analyze the time series of chaotic laser, and figure 6(b) shows the skewness and kurtosis of the chaotic laser as the pump power. It can be seen that the skewness and kurtosis of the chaotic laser fluctuate with the pump power when the pump power range from 70 mW to 120 mW, and the decrease is obvious when the pump power is 85 mW, then fluctuates up and down and tends to be stable when the pump power is 120 mW–150 mW. It can be concluded that the chaotic state reaches its optimal performance at a pump power of 150 mW. The skewness and kurtosis of the chaotic laser exhibit the synchronized trends. The alignment confirms the transition to the randomness of chaotic laser.

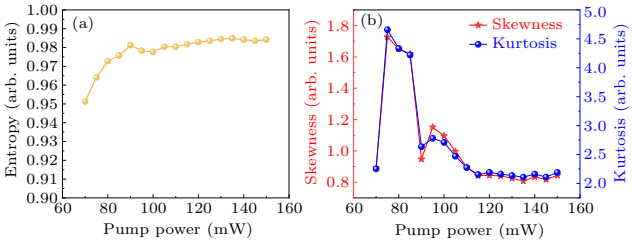


Fig. 6. Complexity analysis of the visible-wavelength chaotic fiber laser: (a) permutation entropy and (b) skewness and kurtosis.

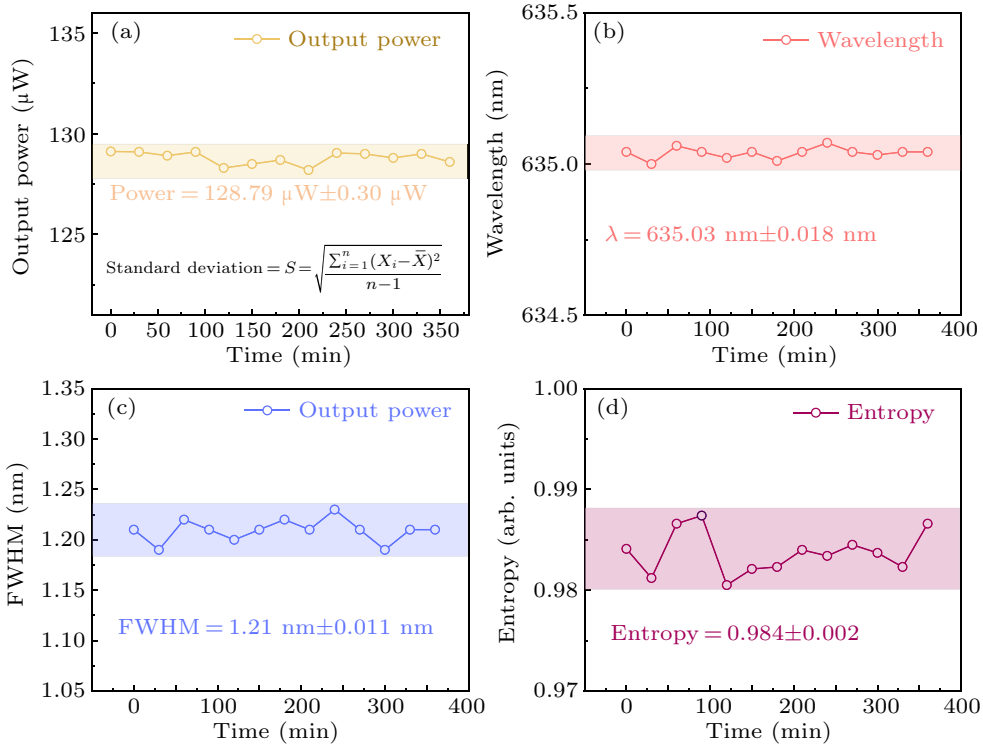


Fig. 7. Stability test of the chaotic fiber laser. Variations of: (a) laser output power, (b) wavelength, (c) FHWM, (d) permutation entropy of the Pr^{3+}/Yb^{3+}-doped fiber laser.

Figure 7 demonstrates the stability of the chaotic laser. Tests were conducted every 30 minutes over a continuous period of 6 hours. Figure 7(a) shows the stability testing of the chaotic laser for the output power. The average power of the laser over 6 hours was 128.79 μW with a power fluctuation of approximately 0.3 μW. Figure 7(b) shows the stability of the wavelength of chaotic laser and the wavelength of the laser has a 0.018-nm fluctuation during the 6 hours test. Figure 7(c) shows the stability of the FWHM of chaotic laser with a maximum fluctuation of 0.011 nm. Figure 7(d) is the permutation entropy of the chaotic laser and it indicate that the permutation entropy of 0.984 is stable, with a fluctuation of no more than 0.002. Compared with biosensing and imaging at near-infrared wavelengths (780 nm–1550 nm), the visible-wavelength chaotic lasers can be applied in biomedical detection.

5. Conclusion and perspectives

We have successfully demonstrated a diode-pumped all-fiber structure chaotic fiber laser operating in the visible wavelength range by 850-nm LD as the pump source. The 4-m long Pr^{3+}/Yb^{3+}-co-doped ZBLAN is used as the gain medium. When the pump power is 120 mW, the laser with the wavelength of 635 nm enters the chaotic state, and the complexity of the chaotic laser increases when the pump power increases. We believe that this approach may also be feasible for other materials for emission in the visible range.

Acknowledgement

Project supported by the National Natural Science Foundation of China (Grant Nos. 61975141, 61575137, and 61675144).

References

[1] Sakuraba R, Iwakawa K, Kanno K and Uchida A 2015 *Opt. Express* **23** 1470
[2] Bouchez G, Malica T, Wolfersberger D and Sciamanna M 2021 *Phys. Rev. E* **103** 042207
[3] Li J, Yang L Z, Ding W J, Zhan M X, Fan L L, Wang J F, Shang H F and Ti G 2021 *Appl. Opt.* **60** 4004
[4] Zhang M and Wang Y 2021 *J. Lightwave Technol.* **39** 3711
[5] Wang L, Mao X, Wang A, Wang Y, Gao Z, Li S and Yan L 2020 *Opt. Lett.* **45** 4762
[6] Annovazzi-Lodi V, Benedetti M, Merlo S, Perez T, Colet P and Mirasso C R 2007 *IEEE Photon. Technol. Lett.* **19** 76
[7] Li X Z, Li S S and Chan S C 2017 *IEEE Photon. J.* **9** 1505411
[8] Uchida A, Amano K, Inoue M, Hirano K, Naito S, Someya H, Oowada I, Kurashige T, Shiki M, Yoshimori S, *et al.* 2008 *Nat. Photon.* **2** 728
[9] Wang D, Lei Y, Shi P and Li Z 2023 *Chin. Phys. B* **32** 090505
[10] Tian J, Yang L, Qin C, Wu T, Wang J, Zhang Z, Li K and Copner N J 2020 *IEEE Sens. J.* **20** 4215
[11] Li M, Zhang X, Zhang J, Zhang M, Qiao L and Wang T 2019 *IEEE Photon. Technol. Lett.* **31** 1389
[12] Chen R, Shu H, Shen B, Chang L, Xie W, Liao W, Tao Z, Bowers J E and Wang X 2023 *Nat. Photon.* **17** 306
[13] Feng L, Gao H, Zhang J, Yu M, Chen X, Hu W and Yi L 2021 *Opt. Express* **29** 719
[14] Tseng C H, Funabashi R, Kanno K, Uchida A, Wei C C and Hwang S K 2021 *Opt. Lett.* **46** 3384
[15] Liu B, Jiang Y and Ji H 2022 *Photonics* **9** 450
[16] Guo Y, Wang D, Wang L, Jia Z, Zhao T, Chang P, Wang Y and Wang A 2023 *Photonics* **10** 370
[17] Xue C P, Wang X, Zheng L K, Zhang H Y, Hong Y H and Zhang Z X 2025 *Chin. Phys. B* **34** 030504
[18] Li J, Yang L, Hao Y, Feng H, Ding W, Wang J, Shang H and Ti G 2024 *Opt. Express* **32** 12496
[19] Wang C, Li J, Zhou X, Cheng Z, Qiao L, Xue X and Zhang M 2023 *Light Sci. Appl.* **12** 213
[20] Zhu J Y, He Z M, Huang C, Zeng J, Lin H C, Chen F C, Yu C Q, Li Y, Zhang Y T, Chen H T and Pu J X 2024 *Chin. Phys. B* **33** 080701
[21] Zou J, Kang Z, Wang R, Wang H, Liu J, Dong C, Jiang X, Xu B, Cai Z, Qin G, Zhang H and Luo Z 2019 *Nanoscale* **11** 15991
[22] Kowalska M, Klocek G, Piramidowicz R and Malinowski M 2004 *J. Alloys Compd.* **380** 156
[23] Demaimay J, Kifle E, Loiko P, Pau F, Recoque G, Georges T, Rault T, Bodin L, Joulain F, Camy P and Braud A 2024 *Opt. Lett.* **49** 4174
[24] Wang H, Zou J, Dong C, Du T, Xu B, Xu H, Cai Z and Luo Z 2019 *Opt. Lett.* **44** 4423
[25] Zhang C, Hong J, Zhou L, Zou J and Luo Z 2023 *Opt. Laser Technol.* **160** 109050
[26] Xie P, Zhao X M, Jain R and Gosnell T R 1998 *Technical Digest. Summaries of Papers Presented at the Conference on Lasers and Electro-Optics*, July 1998 San Francisco, USA, p. 323
[27] Zellmer H, Riedel P and Tünnermann A 1999 *Appl. Phys. B* **69** 417
[28] Zou J, Dong C, Wang H, Du T and Luo Z 2020 *Light Sci. Appl.* **9** 61
[29] Ji S, Wang Z, Huang S, Shen C, Lin J, Xiao B, Feng Q, Xu H and Cai Z 2023 *Opt. Laser Technol.* **158** 108900
[30] Liu S, Lin J, Ji S, Song Y, Feng Q, Xiao B, Wang Z, Xu H and Cai Z 2023 *Opt. Laser Technol.* **157** 108720
[31] Wu D, Peng J, Cai Z, Weng J, Luo Z, Chen N and Xu H 2015 *Opt. Express* **23** 24071
[32] Wu D, Quan C, Guo Z, Cai Z and Xu H 2018 *J. Opt.* **20** 085501
[33] Luo S, Tang X, Geng X, Gu H, Li L and Cai Z 2022 *Opt. Lett.* **47** 5881
[34] Li T, Wang Z, Zou J, Hong J, Ruan Q, Wang H, Dong Z and Luo Z 2023 *Photon. Res.* **11** 413
[35] Lord M P, Olivier M, Bernier M and Vallée R 2023 *Opt. Lett.* **48** 3709
[36] Luo L, Tee T and Chu P 1998 *J. Opt. Soc. Am. B* **15** 972
[37] Abarbanel H D, Kennel M B, Buhl M and Lewis C T 1999 *Phys. Rev. A* **60** 2360